Materials Characterization 172 (2021) 110847

Contents lists available at ScienceDirect

Materials Characterization

journal homepage: www.elsevier.com/locate/matchar

Microstructure and wear characteristics of in-situ micro/nanoscale niobium carbide reinforced copper composites fabricated through powder metallurgy

Yu Bian [a], Junjie Ni [a,b,*], Chao Wang [c], Jinming Zhen [a], Hongguo Hao [d], Xiangjin Kong [d], Hui Chen [a], Jian Li [a], Xiaoqiang Li [a], Zhengfeng Jia [a], Wei Luo [e], Zhong Chen [b,**]

[a] School of Materials Science and Engineering, Liaocheng University, Liaocheng 252059, China
[b] School of Materials Science and Engineering, Nanyang Technological University, Singapore 639798, Singapore
[c] Lanzhou Institute of Chemical Physics, Chinese Academy of Sciences, Lanzhou 730000, China
[d] School of Chemistry and Chemical Engineering, Liaocheng University, Liaocheng 252059, China
[e] State key Lab of Silicon Materials, Zhejiang University, Hangzhou 310027, China

ARTICLE INFO

Keywords:
Cu-matrix composites
In-situ
Carbide
Wear
TEM
XPS

ABSTRACT

In this work, a highly wear-resistant cooper matrix composite reinforced by in situ formed nano-NbC particles was synthesized by hot pressing mechanically alloyed Cu+Nb+C powders. The composite possesses a smaller friction coefficient and displays a wear rate (2.6×10^{-5} mm^3N^{-1} m^{-1}) two orders of magnitude lower than the micro-NbC reinforced Cu composites (123.5×10^{-5} mm^3N^{-1} m^{-1}). Such property enhancement is attributed to the hardness improvement and the solid lubricating effects induced by nanoscale niobium carbides/oxides as well as iron oxides. The oxidation and pulverization of NbC during friction have played a key role in increasing the wear resistance and their mechanisms are discussed. The findings provided a strategy for developing other wear-resistant composite materials.

1. Introduction

Copper matrix composites are important engineering materials and have the potential for applications in electrical sliding contacts that are key components for the homopolar machines or the railway overhead current collector systems [1–3], because they are able to combine high electrical/thermal conductivity of the Cu matric and good mechanical wear resistance of the reinforcing phase. To realize excellent wear resistant properties and high hardness, carbon materials reinforcement (graphite [4], graphene [5–8], carbon nano-tube [9]) and non-metallic reinforcing particles, like oxides (ZrO_2, SiO_2, La_2O_3, TiO_2, Al_2O_3 [10–14]), borides (TiB_2, ZrB_2 [15–17]), sulfides (WS_2, MoS_2 [18,19]) and carbides (SiC, WC, NbC, TiC, B_4C [20–26]) are often added into the matrix. Among the two types of strengthening phases, the second one is more beneficial to hardness. Here the additive NbC is an important candidate to reinforce Cu-based materials because of its extremely high hardness, high melting temperature and good wettability with copper. Usually, its additions are achieved via in or ex situ methods, in which the former directly synthesize NbC using chemical reaction between raw materials [27–30]. The in situ formed reinforcing particles distribute more evenly in the matrix and they have a stronger reinforcement-matrix interfacial bonding than the ex situ method. Therefore, in situ processing is suitable for generating better mechanical properties such as wear resistance and hardness for the Cu-matrix composites. For such materials, the aforementioned properties closely relate to the reinforcement size, too. Generally, the refinement of reinforcing particles increases the hardness, which can decrease the contact area of wear surface and accordingly benefit the abrasion resistance [31]. As the reinforcing particles was refined from micro to nanoscale size, the wear mechanism changes from ploughing to grooving, leading to the pronounced reduction in wear loss [32]. Thus, in situ synthesis of nanoscale NbC made from nanocrystalline powder is a promising strategy for preparing highly wear-resistant Cu-matrix composites.

At present, it is hard to obtain this bulk material by a conventional powder metallurgy route involving powder preparation, compaction and sintering, considering that the nano-grains are prone to grain

* Corresponding author at: Junjie Ni, School of Materials Science and Engineering, Liaocheng University, Liaocheng 252059, China.
** Corresponding author.
E-mail addresses: nijunjie@lcu.edu.cn (J. Ni), ASZChen@ntu.edu.sg (Z. Chen).

https://doi.org/10.1016/j.matchar.2020.110847
Received 29 October 2020; Received in revised form 18 December 2020; Accepted 21 December 2020
Available online 25 December 2020

growth to microscale during sintering [33]. To overcome this problem, Ni et al. [34,35] prolonged mechanical alloying processes of powders to achieve an average size of ~10 nm and then hot pressed the resulting powders with the matrix. Such method was found to have successfully fabricated nanosized TiC and WC strengthened Cu-matrix composites. Inspired by the in situ reaction method, this paper explores the preparation of Cu-matrix composites reinforced by in situ nano-NbC particles. So far, the related information about the fabrication and microstructure of the in situ nanosized niobium carbide reinforced copper matrix composites remains unavailable in the literatures, although there are a few reports on their wear resistance. In the present work, thus, we aimed to produce in situ nanosized NbC reinforced copper matrix composites via hot pressing the mechanically alloyed powders of Cu+Nb+C and investigate the materials structure- property relationship with emphasis on the tribological characteristics.

2. Experimental

Raw materials included copper powder (purity: 99.9%, particle size: ~10 μm), niobium powder (purity: 99.9%, particle size: ~10 μm), and graphite powder (purity: 99%, particle size: ~5 μm) were obtained from Shanghai Naiou Nano Technology Co., Ltd. Morphology and particle size distribution of the raw powders was presented in Fig. 1. A mixture of Cu-15.655wt.%Nb-2.020wt.%C, corresponding to Cu-20 vol% NbC, was ball milled in stainless steel vacuum tanks on a planetary mill for 60 h, 84 h, 96 h, and 120 h. Ball milling (BM) was operated at a rotating speed of 350 rpm and the ball-to-powder weight ratio was maintained at 10:1. During milling, 1.5 wt% stearic acid and 1 wt% ethanol were utilized as the process control agents (PCA) to prevent the re-welding and promote the fracture of powder particles. After the BM process, the resulting powders were sintered by hot pressing at 950 °C for 1 h using silicon

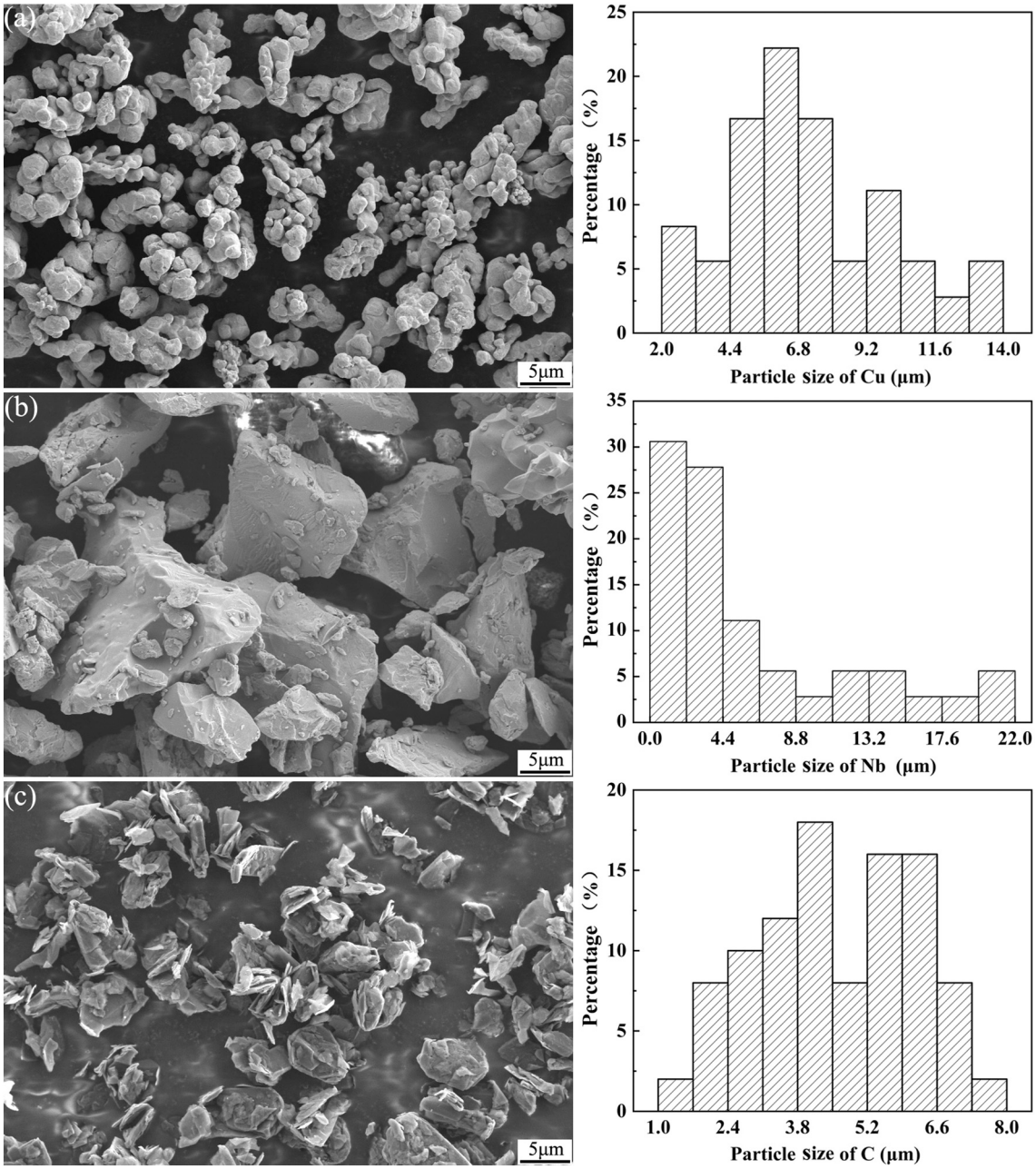

Fig. 1. SEM images and particle size distribution of raw powders of Cu (a), Nb (b), and C (c).

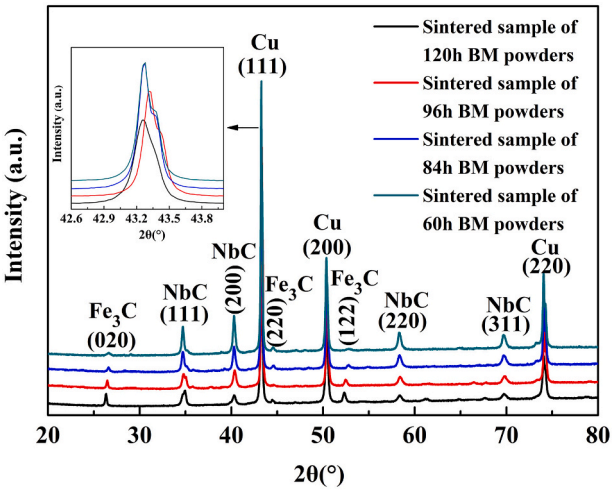

Fig. 2. XRD patterns of sintered samples.

nitride die and punches. The chamber was under vacuum (~4.5×10^{-4} Pa) and a pressure of 100 MPa during the sintering process. The hot-pressed (HP) samples are denoted as x h-BM HP where x represents the ball milling time in hours (x = 60, 84, 96, 120).

Crystalline phase identification and the composition analysis of sintered samples were investigated using an X-ray diffractometer with Cu-Kα radiation and the energy dispersive spectrometer (EDS), respectively. Morphology of un-milled powders and sintered samples was observed by a scanning electron microscope (SEM). High resolution transmission electron microscopy (HRTEM) was carried out on the HP nanocomposites to study the crystalline state of nano-constituents and the matrix-reinforcement interface. For the HP samples, the density was determined by the Archimedes principle. Hardness was measured using a Vicker's microhardness tester with a load of 1.96 N and a loading time of 15 s. Each sample was measured ten times and the average was reported together with the standard deviation. Electrical conductivity measurement was performed on a FQR7501A-typed eddy current conductivity instrument.

Dry sliding wear tests were carried out on an MFT-EC4000 reciprocating friction and wear tester at room temperature. Friction and wear measurements, in which GCr15 steel ball with a 6 mm diameter was

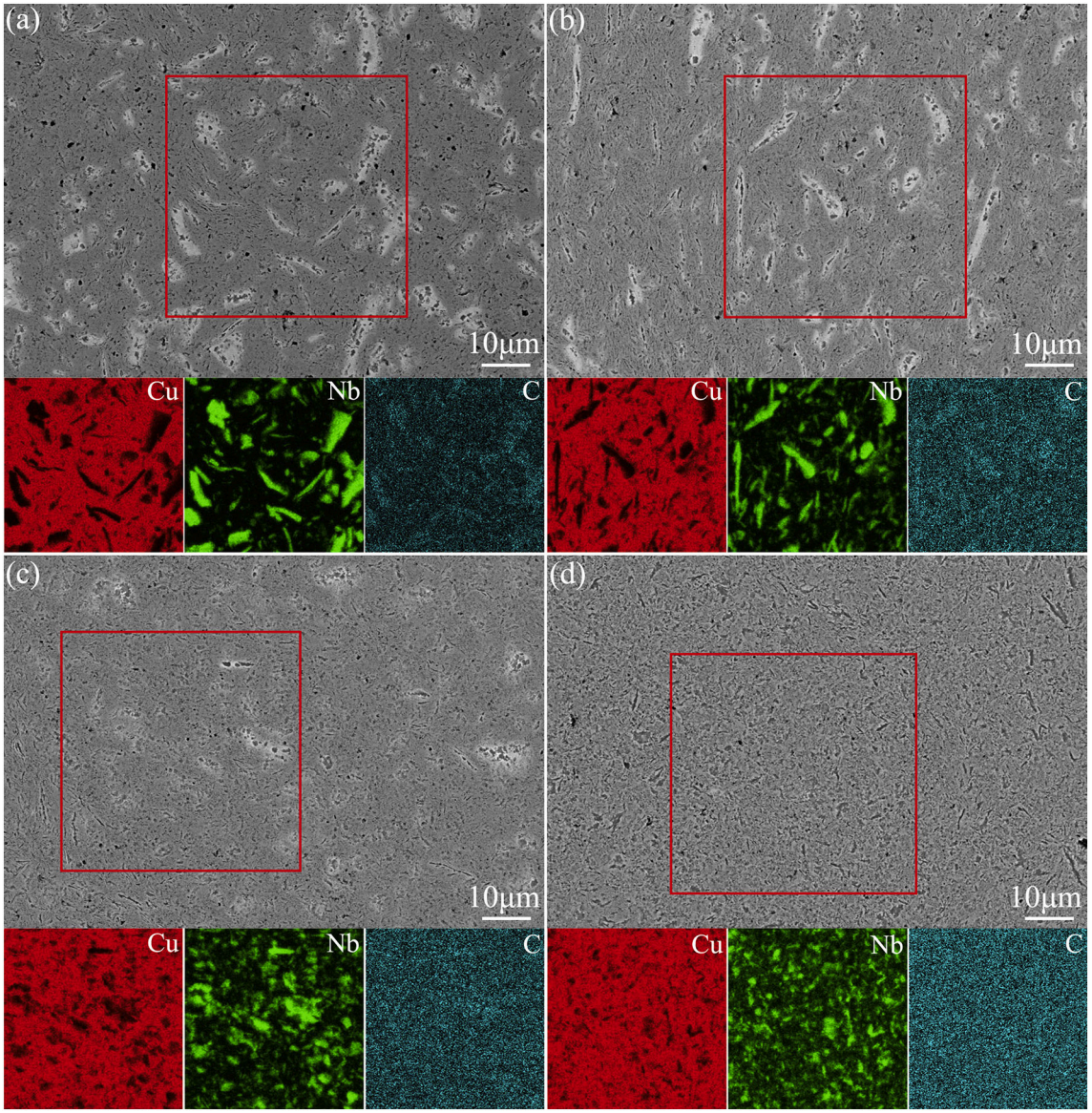

Fig. 3. SEM images and EDS mappings of Cu, Nb and C for the sintered samples from different time BM powders: (a) 60 h, (b) 84 h, (c) 96 h, and (d) 120 h.

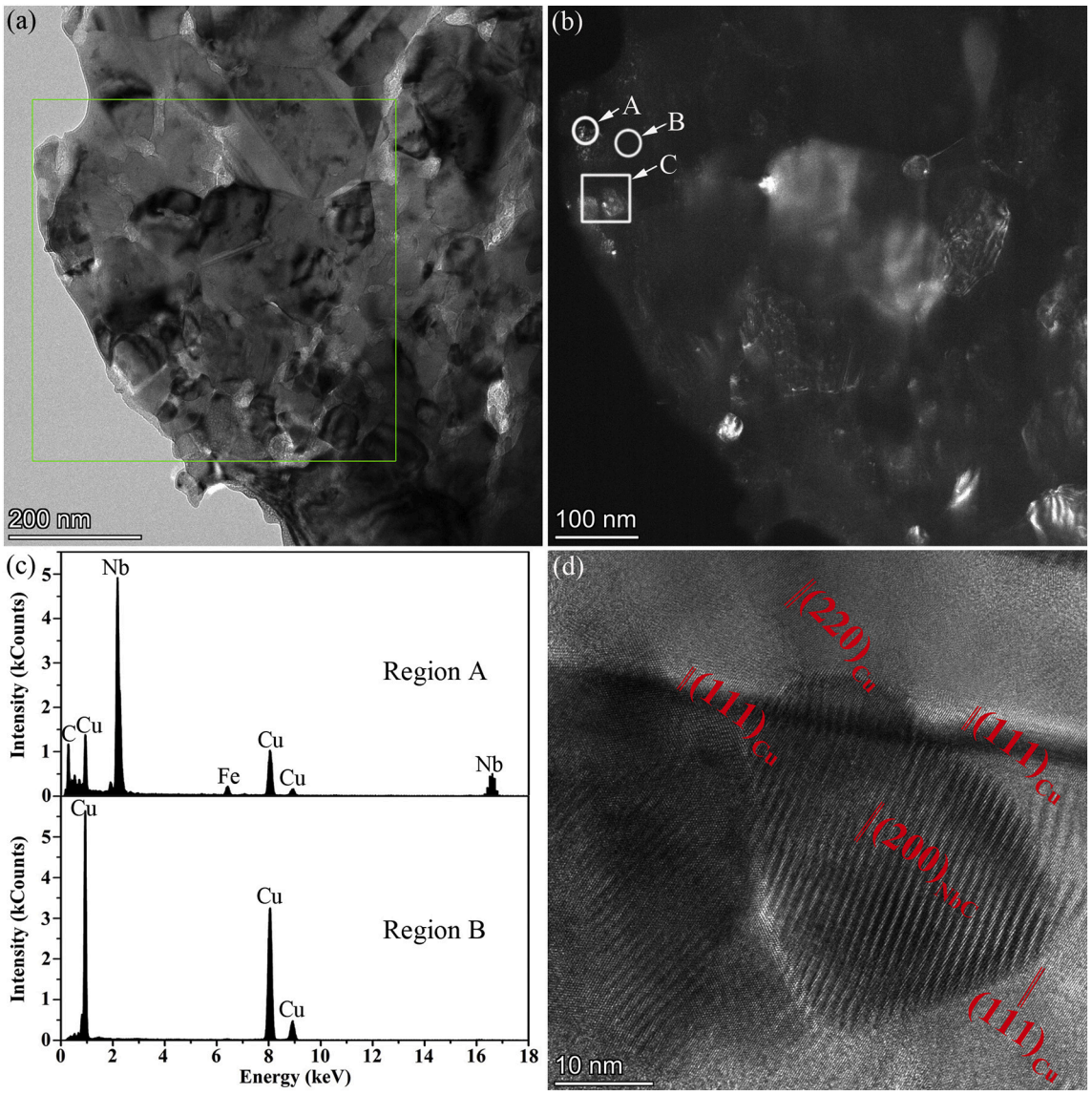

Fig. 4. TEM and EDS for the 120 h-BM HP: (a) Bright field image; (b) Dark field image of the selected area marked by green square; (c) EDS of the regions A and B in dark field image; (d) High-resolution TEM image corresponding to the region C marked by white square. (For interpretation of the references to colour in this figure legend, the reader is referred to the web version of this article.)

used as a counter-sample, were conducted at a load of 2 N, 5 N and 10 N with the sliding distance of 21.6 m and the sliding speed of 12 mm/s. For the worn samples, the morphological characterization of the wear track, as well as the wear debris was analyzed using SEM. The composition analysis was done using EDS mapping and X-ray photoelectron spectrometer (XPS). Al K_α was used as the X-ray source and the XPS depth profiling was performed by sputtering Ar ions. Wear track depth and cross-sectional area (A) were determined by the surface profile of the wear track using 3D optical surface profilometer (OSP). Three different positions were measured in the wear track for the cross-section area of each sample condition, and their average value (A) along with the wear track length (L) was used to calculate the wear volume loss (V_{loss}) in mm^3 according to Eq. (1). $V_{loss}$was normalized by the applied load (N) in N and the total sliding distance (S) in m and expressed as wear rate (W, $mm^3N^{-1}\ m^{-1}$) in Eq. (2).

$$V_{loss} = A \times L \tag{1}$$

$$W = \frac{V_{loss}}{N \times S} \tag{2}$$

Table 1
Hardness, electrical conductivity and relative density of sintered samples.

Sample	Microhardness (Hv)	Electrical conductivity (% IACS)	Relative density (%)	Porosity content (%)
60 h-BM HP	117.9±5.8	30.0±1.4	96.3±1.0	3.7
84 h-BM HP	132.3±4.0	28.4±1.0	94.8±0.8	5.2
96 h-BM HP	164.5±5.0	27.7±1.2	94.3±0.7	5.7
120 h-BM HP	180.0±6.3	25.5±1.0	93.1±0.9	6.9

3. Results and discussion

3.1. Microstructure, hardness and electrical property of the sintered samples

XRD patterns in Fig. 2 show that all samples are composed of Cu and

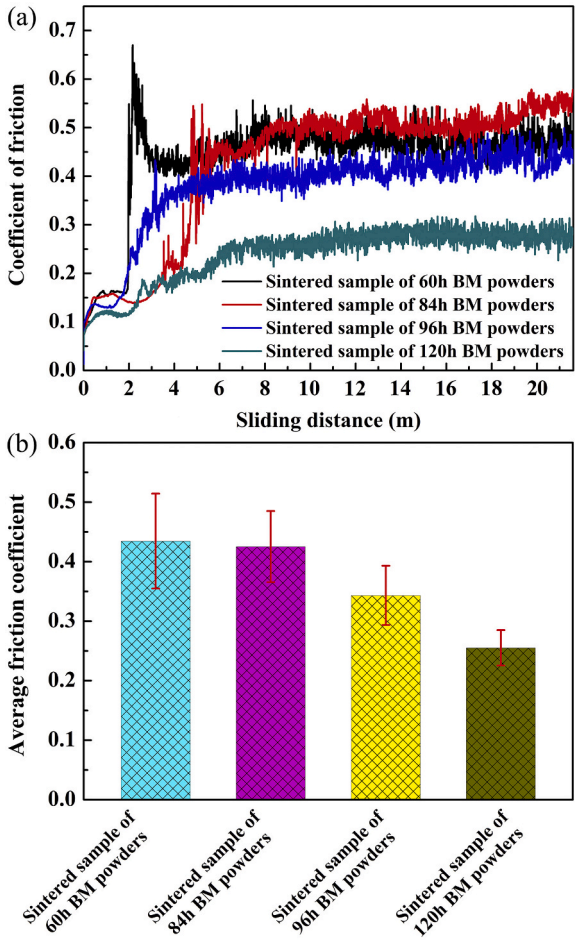

Fig. 5. Friction curves vs. distance (a) and average friction coefficient (b) of the sintered samples.

NbC except for a few cementite, in which such carbides formed directly from the reactions of Nb+C→NbC and 3Fe+C→Fe_3C, respectively under the hot-pressing conditions (950 °C, 100 MPa). The introduction of Fe element was unavoidable in the BM processes. The niobium carbide reached about 20 μm and agglomerated in the 60 h-BM HP while its size was reduced below ~10 μm with a more uniform distribution in 84 h-BM HP, as shown in Fig. 3 in which the EDS mappings of Nb element corresponded to the distribution of NbC. In the 96 h-BM and 120 h-BM HP samples, especially in the latter, NbC distributed very evenly and its size was too small to be measured under SEM. The 120 h-BM HP was thus studied using TEM and the results are displayed in Fig. 4. Based on the TEM observation, most NbC particles were smaller than ~40 nm. The in situ precipitated NbC appeared to effectively pin the grain boundaries of matrix phases (Fig. 4d) and accordingly hindered their grain growth during sintering by the Zener effect [36]. It accounted for the occurrence of nanocrystalline or ultrafine copper matrix in the 120 h-BM HP, in which the Cu matrix phase was much finer compared to the 60 h-BM HP, as proved by the broadening of the Cu (111) peak between 43.0° and 43.7° for the former sample (inset in Fig. 2). Moreover, as observed from Fig. 4 b and c, nanosized Fe_3C coexisted with NbC and it played a similar role in influencing the microstructure of Cu-matrix composites. Such structural variations led to higher fine-grain strengthening of copper matrix phases and better dispersion strengthening of NbC in the sintered compacts of longer-term BM powders. It pronouncedly increased the mean hardness values from 117.9 Hv for the 60 h-BM HP to that of 180.0 Hv for the 120 h-BM HP (Table 1), although the relative density decreased with the milling duration due to the powder refinement. These finer particles tend to possess a lower flow rate, higher specific surface area, higher amount of absorbed gases, and severer inter-particle friction [38], increasing the porosity in the sintered sample. The observed hardening with BM time indicates that the increased porosity had a less impact on the hardness than particle refinement. The increased porosity was responsible for the 15.0% reduction (from 30.0 to 25.5% IACS) in the electrical conductivity. In the present work, the NbC reinforced Cu-matrix composites have higher hardness than the reported Cu-30 vol% NbC fabricated through a conventional sintering [29], because the former was denser and possessed a more optimized microstructure.

3.2. Friction and wear behaviors of the in-situ NbC reinforced Cu composites

The difference in the microstructure and hardness affected the friction and wear behaviors of the in-situ NbC reinforced Cu composites. The friction curves measured at 5 N load are presented in Fig. 5a, and the average friction coefficients are presented in Fig. 5b. All the coefficients of friction (COF) initially increased with the sliding distance and then stabilized for a short distance before ~2 m, due to the formation of stable tribo-layers. Over ~2 m, COF for the 60 h-, 84 h- and 96 h-BM HP samples, especially for the 60 h sample sharply increased owing to ploughing of surface asperities before it became relatively stable against sliding distance. The average values of COF decreased from 0.43 for the 60 h-BM HP to 0.25 for the 120 h-BM HP. The 41.9% COF reduction indicates a much reduced frictional force with the power BM time of composites. This is attributed to the decline of surface roughness induced by the decreased size and more homogenized distribution of NbC in the composites. The uniform distribution of nano-NbC particles in the 120 h-BM HP is responsible for its gentle rise of COF at 2–7 m sliding distance. In addition, the wear rates obtained from the data in the 3D OSP images of wear track with depth profile (Fig. 6) are shown in Fig. 7. It is observed that as compared to 60 h-BM HP, 84 h-BM HP had smaller width and depth of the wear track, due to its higher hardness and smaller NbC particles. Similar reasons account for the further reduced wear for the 96 h-BM HP, and the narrowest and shallowest wear track was observed in the 120 h-BM HP. According to Eqs. (1)–(2), the lower track width and depth means smaller volume wear loss that in turn is

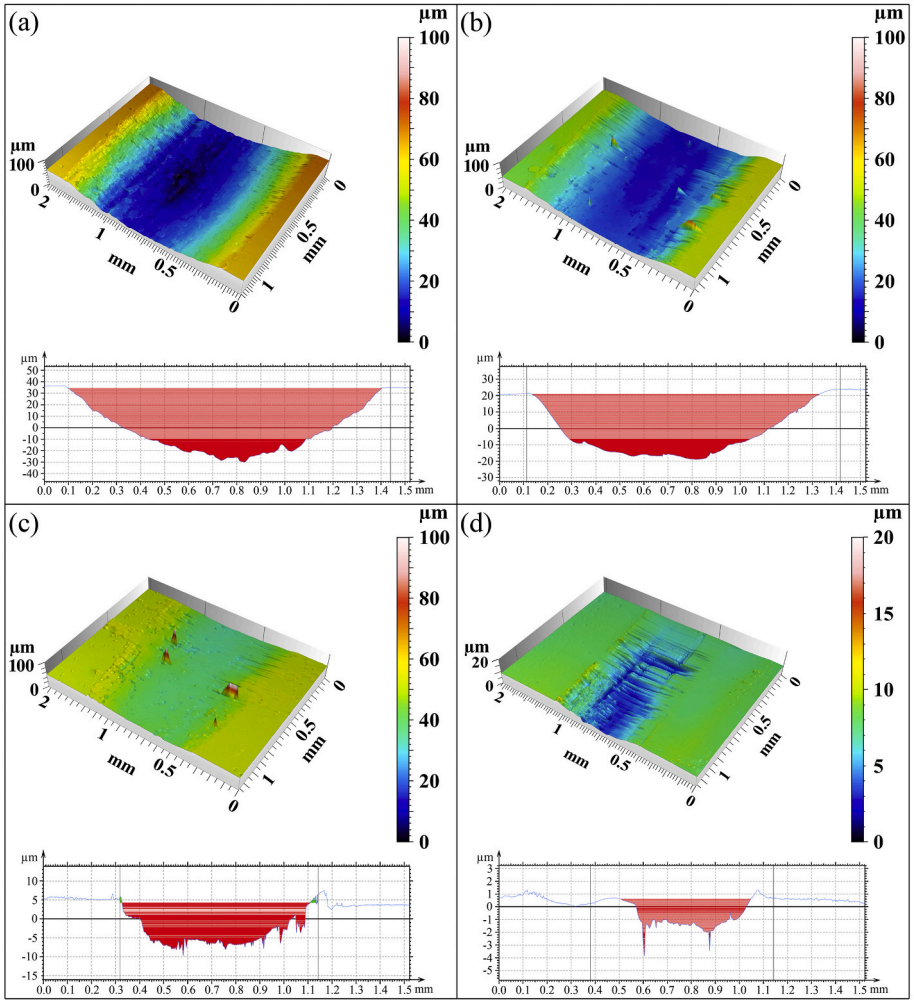

Fig. 6. 3D OSP images with depth profile of wear scar under 5 N load for the sintered sample from different time BM powders: (a) 60 h, (b) 84 h, (c) 96 h, and (d) 120 h.

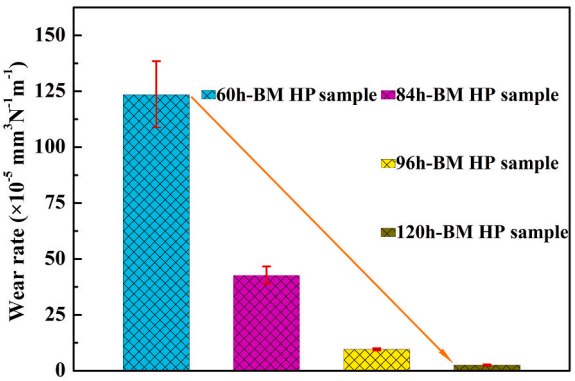

Fig. 7. Comparison of the wear rate under 5 N for the 60 h-, 84 h-, 96 h- and 120 h-BM HP samples.

proportional to wear rate. It thus is easy to understand that the 120 h-BM HP exhibited the smallest wear rate of 2.6 × 10^{-5} mm^3N^{-1} m^{-1}, which had been reduced by two orders of magnitude from the value of 123.5 × 10^{-5} mm^3N^{-1} m^{-1} for the 60 h-BM HP. The best-performing 120 h-BM HP possessed the highest anti-wear property due to its most uniformly distributed nano-NbC particles together with the formation of strong coherent interfaces with the matrix, which has most effectively inhibited particle pull-out during wear test [37].

The particles size in the 60 h- and 120 h-BM HP samples is in the micro and nanoscale, respectively. They were chosen to investigate the load effect on the wear characteristics of Cu-matrix composites. Both

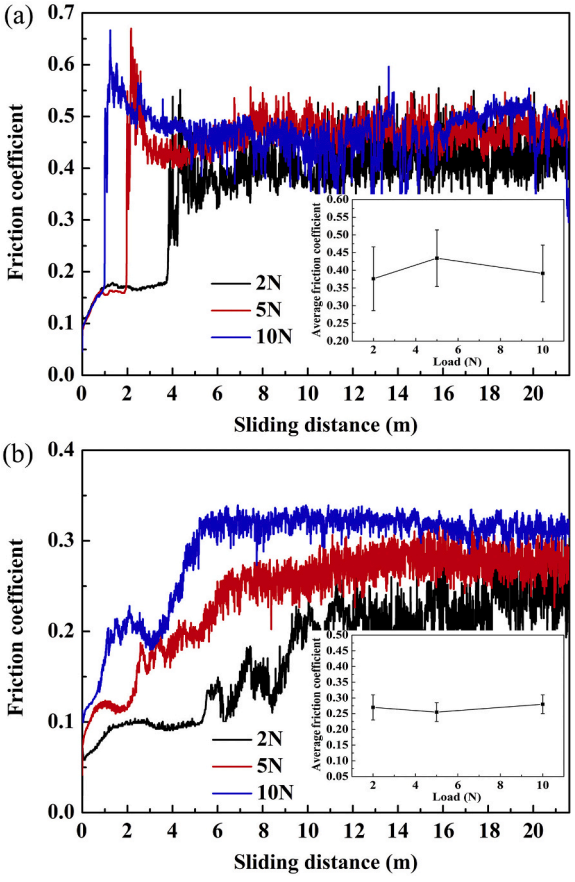

Fig. 8. Friction curves and average friction coefficient under different load for the 60 h-BM HP (a) and120 h-BM HP (b).

samples' friction curves at 2 N and 10 N loads were compared with the case of 5 N (Fig. 8) and their 3D OSP images of wear track along with the depth profile are given in Fig. 9. Clearly, the 120 h-BM HP showed much lower average values at different loads as compared to that of 60 h-BM HP, due to its fine-grained microstructure with large density of dislocations network [38]. For the former sample, the average COF had almost the same values, implying that the friction surface roughness never changed with the increase in the loads. For the latter sample, the increase of average friction coefficient with loads at 2–5 N indicates the coarse surfaces appeared under the frictional load of 5 N. Further increase of loads from 5 to 10 N, however, made the friction surfaces smooth as indicated by the decreased COF (inset in Fig. 8a). Observation of Figs. 6a, d and 9 shows an increase in the wear track width and depth with the load for the composites with both micro and nanoscale NbC. This can be explained on the basis of the proportional relationship between wear volume loss and load [39]. In the load range from 2 to 5 N, sever wear through ploughing was found in the 60 h-BM HP, as validated by a 208% increment of the wear rate (Fig. 10). But this rate had only been increased by 9.8% at 5–10 N and it hardly changed with the applied loads in the 120 h-BM HP. This is related with the comminution of reinforcing phases during wear and will be discussed next.

3.3. Mechanism of NbC reinforcing phase on wear

Results mentioned above indicate that the tribological properties are closely related with the size and distribution of NbC particles. In order to address the mechanism of both structural parameters on wear behaviors, SEM morphologies of worn surfaces and wear-debris along with their EDS and XPS data are presented in Figs. 11–14. As shown in Fig. 11b, the worn surface of 60 h-BM HP was covered by a loose layer, which appeared to be the agglomerate of fine powder-like and large flake-like particles. This features remained in 84 h- and 96 h-BM HP samples as well, in addition to the existence of some relatively smooth regions. Such wear scar features suggest that adhesive wear dominated the wear mode of these three samples. In 120 h-BM HP, the fluffy particulate-agglomerate layers disappeared completely and the worn surfaces became compact and smooth. Coupled with the cutting lines, the wear mode of this composite with nano-NbC was abrasive wear. Furthermore, unlike the first three samples whose debris morphologies are shown in the insets of Fig. 11a, c and e, respectively, the wear-debris of 120 h-BM HP was too small to be collected. Large wear debris (~200 μm size), consisted of flake-like particles appeared in the 60 h-BM HP, in addition to a few of fine, powder-like granules. Similar wear debris were also observed for the 84 h- and 96 h-BM HP samples. In the latter case, the tiny particle debris dominated in number and the size of some relatively large debris was about 60 μm. It thus was stated that smaller wear-debris peeled off the substrate with finer reinforcements in the samples with microscale or mixed micro and nanometer NbC. Both the debris and tribolayers formed in dry-sliding-wear conditions were comprised of materials mixtures from the composite, the counterface, and the environment. The composition analysis indicates a considerable amount of Fe and O as shown in the EDS mappings in Fig. 11, besides Cu, Nb and C that are primary elements of composites. Appearance of Fe revealed the transfer of the counterface materials to the wear surface and the oxygen element suggests oxidation reaction has taken place during the friction and wear experiment. Herein the oxygen tended to combine with iron instead of copper, as implied by the roughly similar element distributions of O and Fe, which is ascribed to a greater level of reactivity of iron under the test conditions. All the aforementioned evidences confirmed the existence of oxidation-delamination in the friction and wear processes.

Comparing the Nb distributions in Figs. 3 and 11, there was a decrease of its clump size in the 60 h-BM and 84 h-BM HP samples before and after frictions, implying the NbC powdering during the friction processes. With the purpose of further elaborating the oxidation reactions along with the role of NbC particles, the chemical and phase composition of tribo-layers for the 60 h-BM and 120 h-BM HP samples

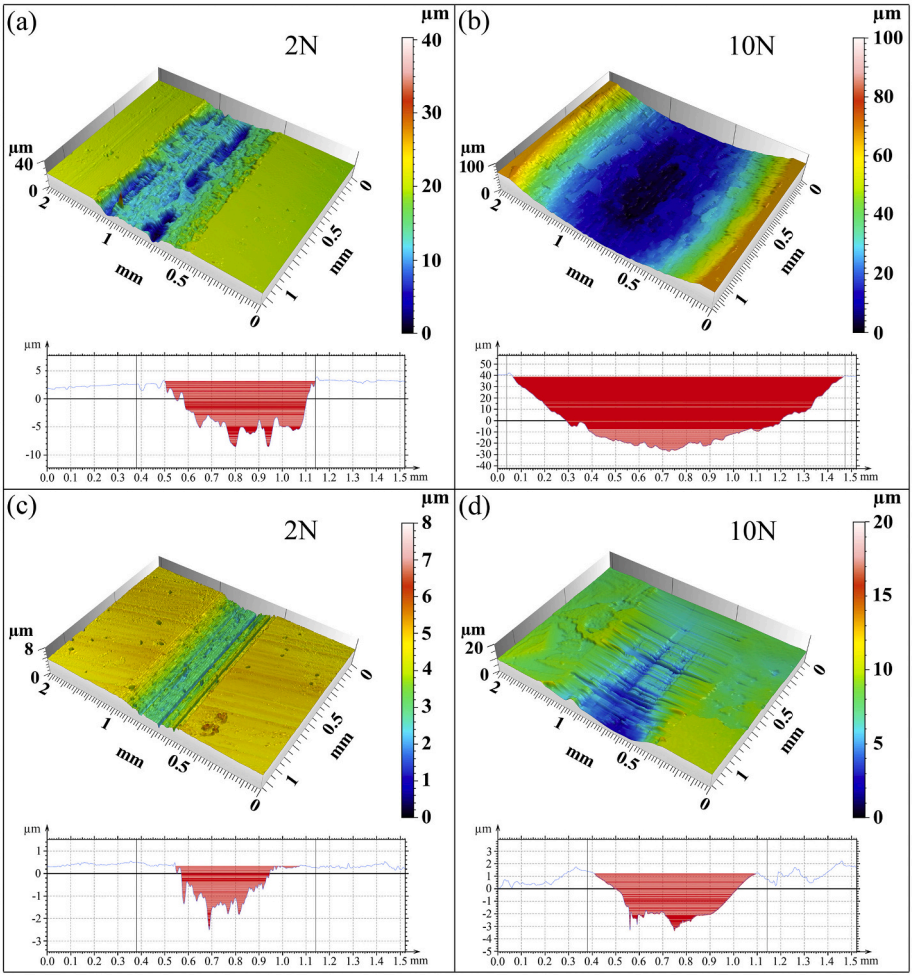

Fig. 9. 3D OSP images with depth profile of wear scar for the 60 h-BM HP (a, b) and120 h-BM HP (c, d) under 2 N and 10 N loads.

were analyzed using XPS, as depicted in Figs. 12 and 13. All the broad survey spectra obtained from 0 to 1200 eV identified the elements of Cu, Fe, Nb, O, and C on the worn layers sputtered after different times of 0–180 s. High-resolution spectra of Cu 2p, Fe 2P, Nb 3d analyzed using mixed Gaussian/Lorentzian functions demonstrate that for the 60 h-BM HP, the worn surfaces contained Cu, Cu_2O, CuO, Fe, Fe_3O_4, Fe_2O_3, NbC, and NbO_2 before sputtering. Among the phases, the presence of the

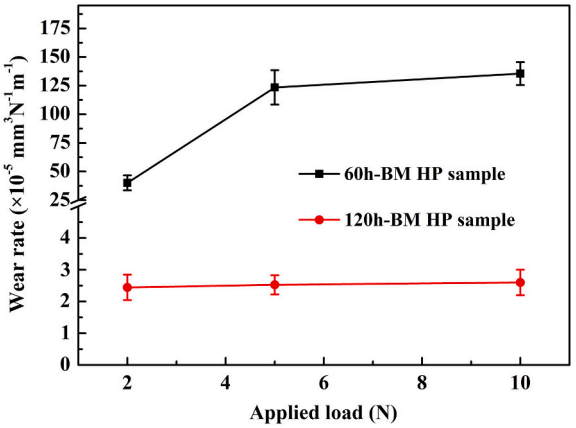

Fig. 10. Changes of the wear rate as a function of applied load for the 60 h-BM HP and 120 h-BM HP.

oxides of iron, copper and niobium indicates that the cooperatively mechanical and thermal actions induced by friction not only provided the sufficient forces for Fe+O and Cu+O reactions that took place in other Cu-based composites [40], but also for NbC+O reaction according to Eq. (3). Besides of NbO_2, Nb_2O_5 was also formed (Eq. (4)), and its phase content increased with the sputtering time from 30 s to 180 s (Fig. 13).

$$NbC + 2O_2 \rightarrow NbO_2 + CO_2 \quad (3)$$

$$NbC + \frac{9}{2}O_2 \rightarrow \frac{1}{2}Nb_2O_5 + CO_2 \quad (4)$$

More Nb_2O_5, whose percentage was obtained by calculating the peak areas of reference spectra of NbO_2, Nb_2O_5 and NbC, was attributed to higher temperature in deeper tribolayers [41]. It should be pointed out that Nb_2O_5 was brittle and this phase with the applied load brought about crack formation in NbC. This might be able to explain the pulverization of NbC phase in the surface layer after friction. Fig. 14 shows that the total niobium oxides in the sputtered layers were less than those of the non-sputtered ones, due to less oxygen exposure in the former. The same reason also accounts for the absence of copper oxidation in the sputtered wear layer (Fig. 12), though a higher temperature would benefit the formation of copper oxides in comparison with the non-sputtered layer. Our observations suggest that the presence of oxygen is probably a more dominant factor than temperature affecting the formation of copper oxides during friction. The temperature factor,

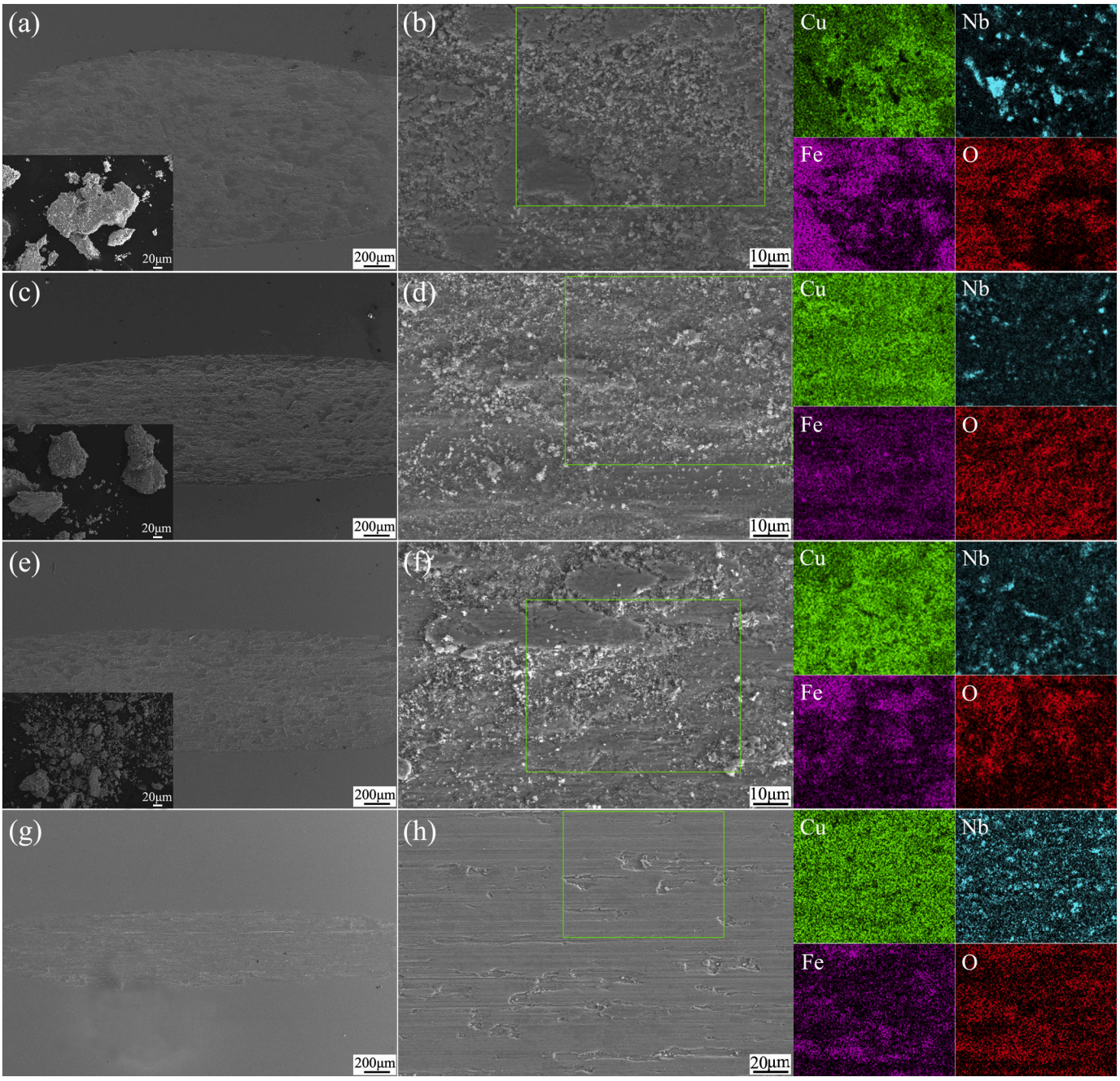

Fig. 11. SEM images on the wear scar under 5 N and wear debris as well as the EDS mappings corresponding to the selected area marked by green square for sintered samples from different time milled powders: 60 h (a, b), 84 h (c, d), 96 h (e, f), 120 h (g, h). (For interpretation of the references to colour in this figure legend, the reader is referred to the web version of this article.)

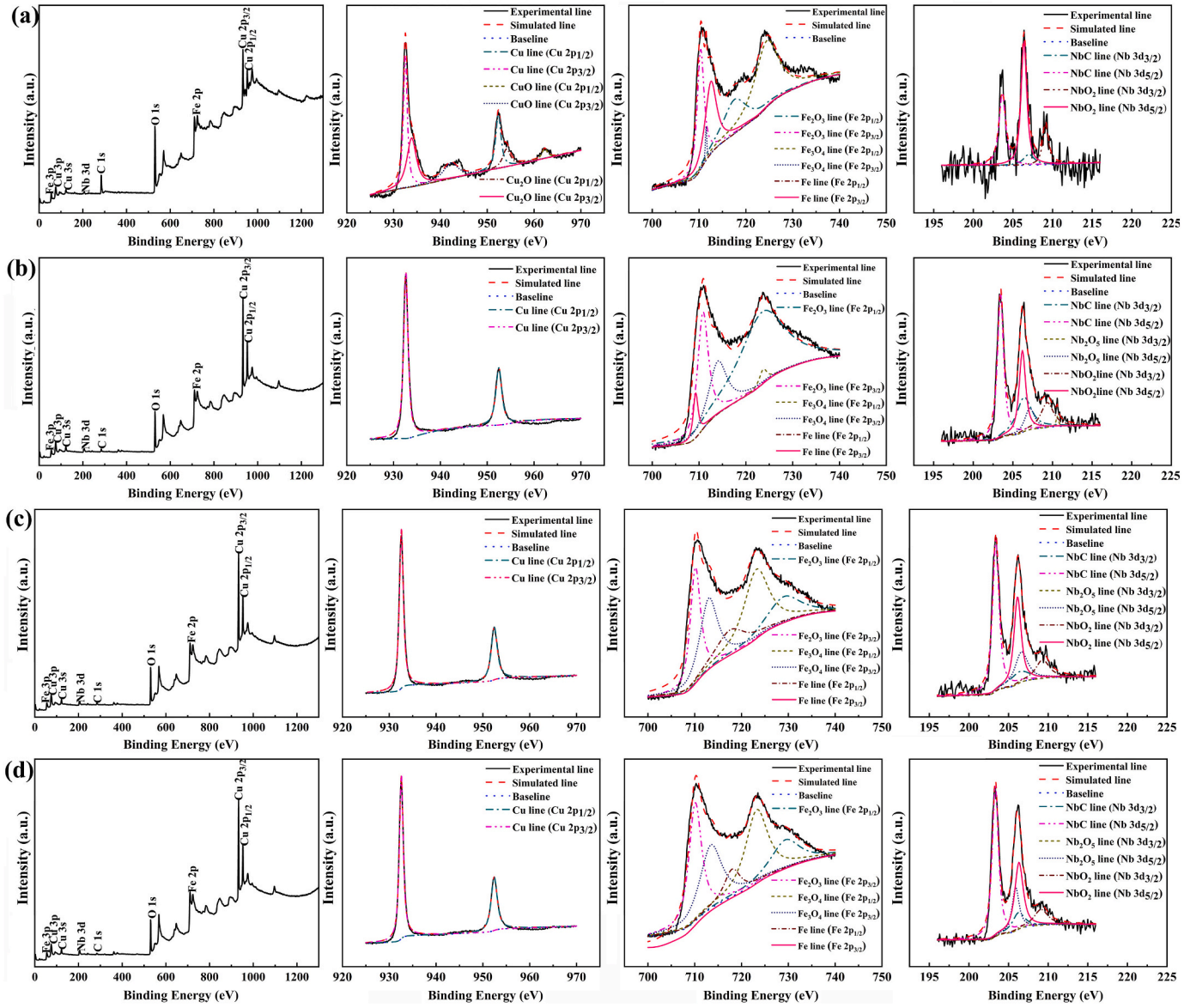

Fig. 12. XPS survey spectrum of the worn surfaces for 60 h-BM HP and its high-resolution spectra of Cu 2p, Fe 2P, Nb 3d at different sputtering time: (a) 0 s, (b) 30 s, (c) 60 s, (d) 180 s.

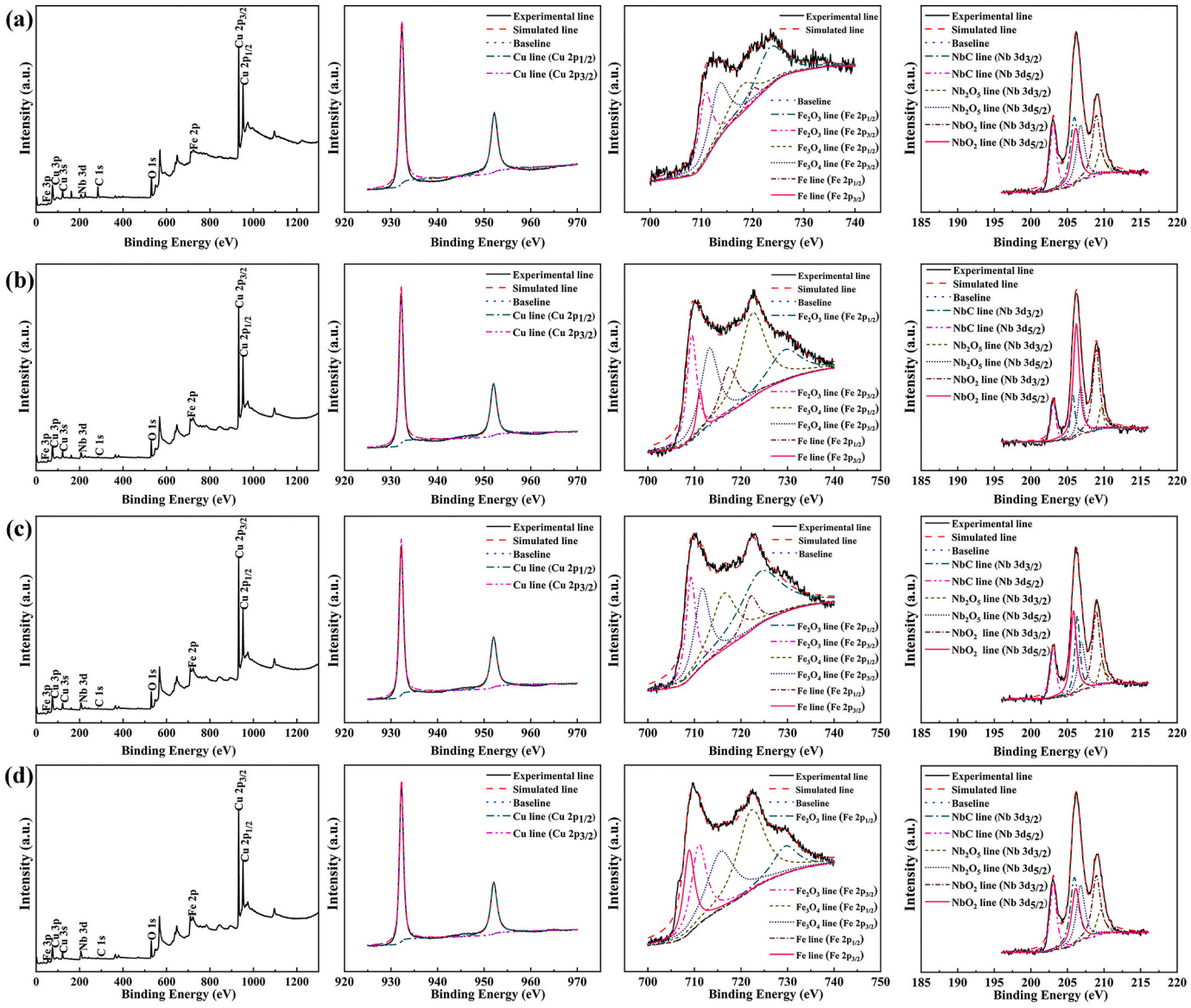

Fig. 13. XPS survey spectrum of the worn surfaces for 120 h-BM HP and its high-resolution spectra of Cu 2p, Fe 2P, Nb 3d at different sputtering time: (a) 0 s, (b) 30 s, (c) 60 s, (d) 180 s.

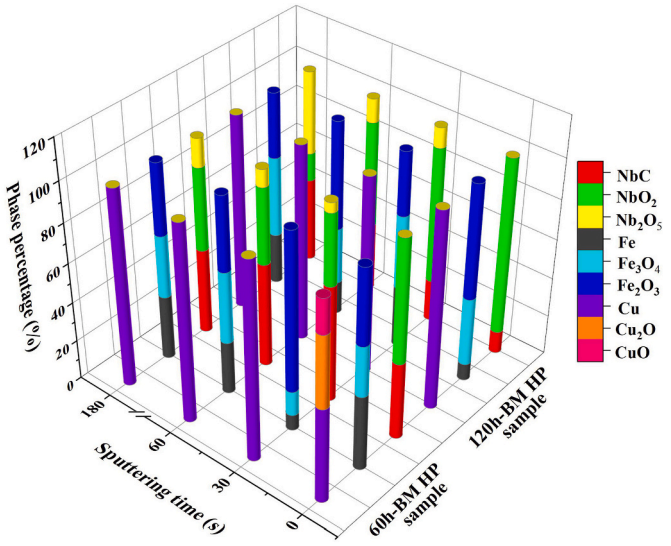

Fig. 14. Phase proportion of oxidation products for Fe+O, Cu+O and NbC+O reactions in the worn layer at different sputtering time for 60 h-BM and 120 h-BM HP.

however, might play a major role in iron oxides formation, as indicated by their smaller amount in the worn layer without sputtering. Compared with the case of 60 h-BM HP, the worn surfaces of 120 h-BM HP had a lower temperature as indicated by its smaller friction coefficient (Fig. 5), explaining the absence of copper oxides on the outermost friction layer. There was a higher proportion of NbO_2, Fe_3O_4 and Fe_2O_3 than the former case, which is ascribed to the decreased sizes of NbC and Fe.

The size reduction of NbC particles from micro to nanoscale means a significant increase in the specific surface area, accordingly enhancing the surface oxidation of NbC. It therefore is easy to comprehend that the tribolayer of the 120 h-BM HP sputtered after 30, 60 and 180 s displayed a larger percentage of Nb_2O_5 than the 60 h-BM HP. The Nb_2O_5 particles can easily break down into nano-Nb_2O_5 and the resulting particles acted as abrasive on the worn surface. Compared with Cu-matrix materials with microscale NbC, the nanoparticles dispersed much more uniformly in the tribolayers, as proven by the Nb EDS mapping in Fig. 11. Coupled with Fe_3O_4 and Fe_2O_3, they are able to produce the solid lubricating effects [42]. Their presence decreased the surface roughness, leading to a lower friction coefficient than in the micro-NbC reinforced composites. On the other hand, the higher hardness imparted these nano-NbC reinforced materials with good wear resistance, because the nanoparticles of niobium carbide/oxides, like nano-TiB_2 particles [3], served to delay the transition to severe wear rate regime.

Furthermore, as a larger load was applied, more severe oxidation and pulverization of NbC would take place due to the generation of more frictional heat during sliding, decreasing the abrasive size of niobium carbide/oxides and accordingly reducing the wear loss and wear rate [40]. It was responsible for the nearly constant wear rate of 120 h-BM HP with load from 2 to 10 N, although larger friction load increased wear loss [24,43]. This is thus concluded that the beneficial effect of reduced abrasive particle size surpassed the harmful effect of a larger load on the wear rate in this composite with nanoscale NbC. Such phenomenon however did not occur in the micro-NbC reinforced composites, as by implied the increased wear rate (Fig. 11). Additionally for the 60 h-BM HP, a far smaller increase in the wear rate under 5–10 N than the case of 2–5 N indicates that microscale NbC oxidized and pulverized more severely with increasing load after 5 N. Larger loads also caused more severe plastic deformation of Cu matrix and Fe counter materials in the composite with micro-NbC, increasing the area percentage of the compact friction films with cracks, as shown Figs. 11b and

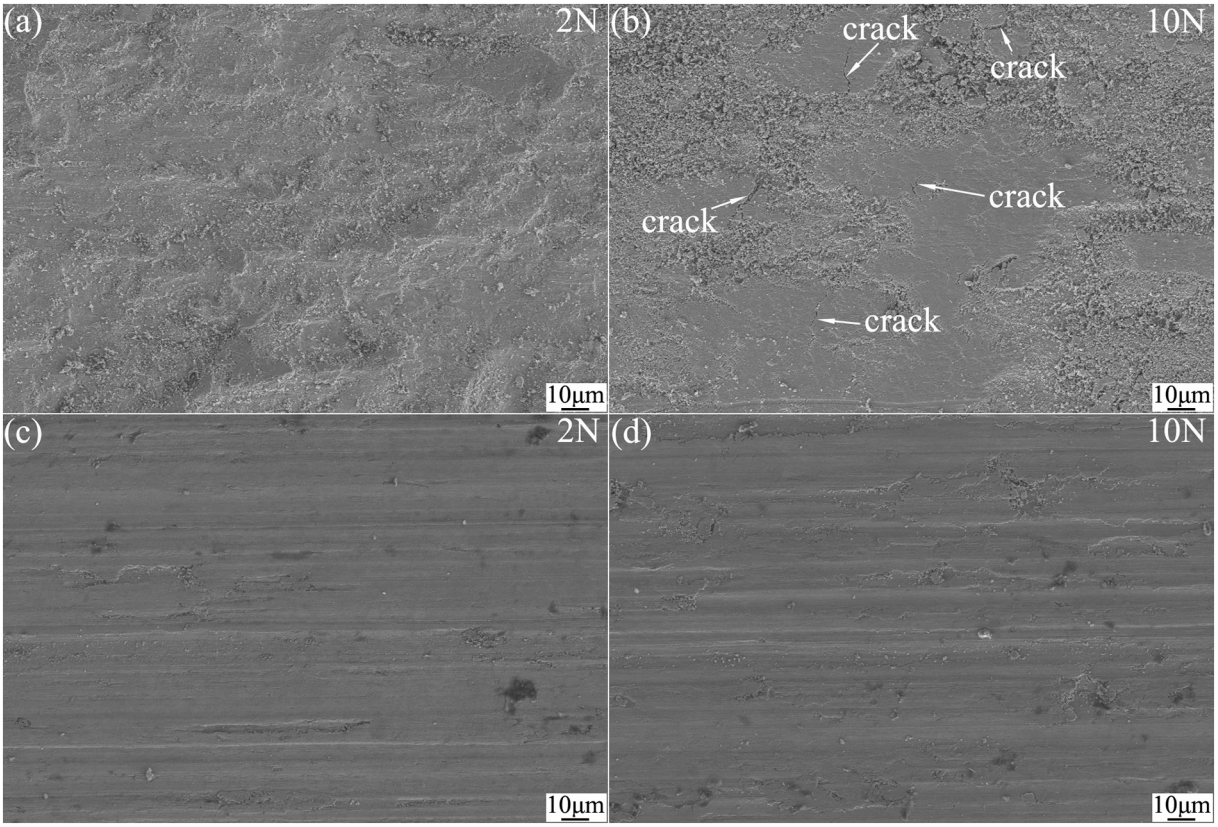

Fig. 15. SEM images on the wear scar of 60 h-BM HP (a, b) and 120 h-BM HP (c, d) under 2 N and 10 N, respectively.

15a–b. In the 120 h-BM HP at different applied loads, the worn surface remained similar topography, that is, the compact and smooth regions, and there only existed trace amount of wear debris (Fig. 15 c and d). This is ascribed to the localized toughening effect of NbC nanoparticles, their migration from the grain boundaries to grain interiors of Cu grains during the friction deformation, [37] and the higher bonding force with the Cu matrix phase than the case of micro-NbC particles. These microscale particles were prone to pull out and the pulled-out ceramic particles will act as abrasive particles themselves, exacerbating the wear of the composites. This partly accounts for their lower abrasion resistance in comparison with the nano-NbC reinforced composite materials.

4. Conclusions

(1) Compared with the composites with micro-NbC, the wear rate had been reduced by two orders of magnitude and the average values of friction coefficients under 5 N load decreased by 41.9% for the nano-NbC reinforced composite. Such enhancement of anti-friction/wear properties was due to the hardness improvement and the solid lubricating effects induced by the nanosized NbC and oxides including Nb_2O_5, NbO_2, Fe_2O_3, and Fe_3O_4.

(2) Nano-NbC reinforcement and its oxidation products were responsible for the abrasive wear mode of the nano-NbC reinforced Cu-matrix composites as compared to the adhesive wear that dominated the wear mode in the micro-NbC containing materials. During friction NbC undergone oxidation, leading to its own pulverization that became more severe with increasing friction load. This explained the nearly unchanged wear rate with the applied loads for the nanoscale NbC reinforced composite.

Declaration of Competing Interest

The authors declare that we have no known competing financial interests or personal relationships that could have appeared to influence the work reported in this paper.

Acknowledgments

The authors wish to thank the support of the Nature Science Foundation of Shandong Province of China under Grant No. ZR2017MEM001, the Zhejiang Provincial Natural Science Foundation of China under Grant No. LY17E010004 and Open Foundation for the State Key Laboratory of Solid Lubrication under Grant No. LSL-1808.

References

[1] H. Zhao, Y. Feng, Z.J. Zhou, G. Qian, J.C. Zhang, X.C. Huang, X.B. Zhang, Effect of electrical current density, apparent contact pressure, and sliding velocity on the electrical sliding wear behavior of Cu-Ti_3AlC_2 composites, Wear 444-445 (2020) 203156.
[2] J.K. Xiao, S.X. Xiao, J. Chen, C. Zhang, Wear mechanism of Cu-based brake pad for high-speed train braking at speed of 380 km/h, Tribol. Int. 150 (2020) 106357.
[3] J.P. Tu, W. Rong, S.Y. Guo, Y.Z. Yang, Dry sliding wear behavior of in situ Cu-TiB_2 nanocomposites against medium carbon steel, Wear 255 (2003) 32–835.
[4] Z. Chen, H.C. Fang, J.M. Zhu, J.W. Li, Y.X. Xu, Z. Sun, F. Chen, P. Xiao, Effect of carbon type and morphology on the microstructure and properties of carbon/copper composites, Wear 460-461 (2020) 203473.
[5] Z.F. Jia, T.D. Chen, J. Wang, J. Ni, H.Y. Li, X. Shao, Synthesis, characterization and tribological properties of Cu/reduced graphene oxide composites, Tribol. Int. 88 (2015) 17–24.
[6] Z.F. Jia, Ha. Li, Y. Zhao, D.A. Dikin, J. Ni, L. Zhao, J. Zhen, B. Ge, X. Shao, F. Ren, Preparation and electrical properties of sintered copper powder compacts modified by polydopamine derived carbon nano films, J. Mater. Sci. 53 (2018) 6562–6573.
[7] Z.F. Jia, H. Li, Y. Zhao, L. Frazer, B. Qian, E. Borguet, F. Ren, D.A. Dikin, Electrical and mechanical properties of poly(dopamine)-modified copper/reduced graphene oxide composites, J. Mater. Sci. 52 (2017) 11620–11629.
[8] Z.F. Jia, P. Zhao, J. Ni, X. Shao, L. Zhao, B. Huang, B. Ge, C. Ban, The electrical conductivities and tribological properties of vacuum hot-pressed cu/reduced graphene oxide composite, J. Mater. Eng. Perform. 26 (2017) 4434–4441.
[9] S.H. Lee, Microstructure and mechanical properties of 3vol%CNT reinforced cu matrix composite fabricated by a powder in sheath rolling method, Korean J. Mater. Res. 30 (2020) 149–154.
[10] H.B. Zhou, P.P. Yao, T.M. Gong, Y.L. Xiao, Z.Y. Zhang, L. Zhao, K.Y. Fan, M. W. Deng, Effects of ZrO_2 crystal structure on the tribological properties of copper metal matrix composites, Tribol. Int. 138 (2019) 380–391.
[11] T.M. Gong, P.P. Yao, X. Xiong, H.B. Zhou, Z.Y. Zhang, Y.L. Xiao, L. Zhao, M. W. Deng, Microstructure and tribological behavior of interfaces in Cu-SiO_2 and Cu-Cr metal matrix composites, J. Alloys Compd. 786 (2019) 975–985.
[12] R. Zheng, N. Li, Z. Zhan, Friction and wear behavior of Cu-La_2O_3 composite sliding against 52100 bearing steel in vacuum, Vacuum 161 (2019) 55–62.
[13] G. Nageswaran, S. Natarajan, K.R. Ramkumar, Synthesis, structural characterization, mechanical and wear behavior of Cu-TiO_2-Gr hybrid composite through stir casting technique, J. Alloys Compd. 768 (2018) 733–741.
[14] W.Y. Tan, X.S. Jiang, Z.Y. Shao, H.L. Sun, T.F. Song, Z.P. Luo, Fabrication and mechanical properties of α-Al_2O_3 whisker reinforced Cu-graphite matrix composites, Powder Technol. 375 (2020) 124–135.
[15] C. Zou, Z. Chen, H. Kang, W. Wang, R. Li, Study of enhance dry sliding wear behavior and mechanical properties of Cu-TiB_2 composites fabricated by in situ casting process, Wear 392–393 (2017) 118–125.
[16] X.L. Fan, X.W. Huang, Q. Liu, H.M. Ding, H.Q. Wang, C. Hao, The microstructures and properties of in-situ ZrB_2 reinforced Cu matrix composites, Results Phys. 14 (2019) 102494.
[17] J. Feng, K.X. Song, S.H. Liang, X.H. Guo, Y.H. Jiang, Electrical wear of TiB_2 particle-reinforced Cu and Cu-Cr composites prepared by vacuum arc melting, Vacuum 175 (2020) 109295.
[18] G. Qian, Y. Feng, Y. Chen, F. Mo, Y. Wang, W. Liu, Effect of WS_2 addition on electrical sliding wear behavior of Cu-graphite-WS_2 composites, Trans. Nonferrous Metals Soc. China 25 (2015) 1986–1994.
[19] Y.Y. Zhang, Y. Epshteyn, R.R. Chromik, Dry sliding wear behaviour of cold-sprayed Cu-MoS_2 and Cu-MoS_2-WC composite coatings: the influence of WC, Tribol. Int. 123 (2018) 296–306.
[20] N.B. Dhokey, R.K. Paretkar, Study of wear mechanisms in copper-based SiC_p (20% by volume) reinforced composite, Wear 265 (2008) 117–133.
[21] Y. Zhang, D. Choudhuri, T.W. Scharf, S. Descartes, R.R. Chromik, Tribologically induced nanolaminate in a cold-sprayed WC-reinforced Cu matrix composite: a key to high wear resistance, Mater. Des. 182 (2019) 108009.
[22] M.R. Akbarpour, H.M. Mirabad, M.K. Azar, K. Kakaei, H.S. Kim, Synergistic role of carbon nanotube and SiC_n reinforcements on mechanical properties and corrosion behavior of Cu-based nanocomposite developed by flake powder metallurgy and spark plasma sintering process, Mater. Sci. Eng. A 786 (2020) 139395.
[23] S.S. Gholami, P. Abachi, K. Pourazarang, M.M. Rahvard, Preparation of in-situ Cu/NbC nanocomposite and its functionally graded behavior for electrical contact applications, T. Nonferr. Metal. Soc. 25 (2015) 863–872.
[24] T. Shi, L. Guo, J. Hao, C. Chen, J. Luo, Z. Guo, Microstructure and wear resistance of in-situ TiC surface composite coating on copper matrix synthesized by SHS and Vacuum-Expendable Pattern Casting, Surf. Coat. Technol. 324 (2017) 288–297.
[25] M.R. Akbarpour, S. Alipour, A. Safarzadeh, H.S. Kim, Wear and friction behavior of self-lubricating hybrid Cu-(SiC+xCNT) composites, Compos. Part B 158 (2019) 92–101.
[26] R. Sathiskumar, I. Dinaharan, N. Murugan, S.J. Vijay, Influence of tool rotational speed on microstructure and sliding wear behavior of Cu/B_4C surface composite synthesized by friction stir processing, Trans. Nonferrous Metals Soc. China 24 (2014) 95–102.
[27] W. Zeng, J.W. Xie, D.S. Zhou, Z.Q. Fu, D.L. Zhang, E.J. Lavernia, In-situ formation of NbC in nanocrystalline Cu, J. Alloys Compd. 725 (2017) 334–341.
[28] Z. Hussain, R. Othman, B.D. Long, M. Umemoto, Synthesis of copper-niobium carbide composite powder by in situ processing, J. Alloys Compd. 464 (2008) 185–189.
[29] H. Zuhailawati, H.M. Salihin, Y. Mahani, Microstructure and properties of copper composite containing in situ NbC reinforcement: effects of milling speed, J. Alloys Compd. 489 (2010) 369–374.
[30] C. Suryanarayana, N. Al-Aqeeli, Mechanically alloyed nanocomposites, Prog. Mater. Sci. 58 (2013) 383–502.
[31] G.H.A. Bagheri, The effect of reinforcement percentages on properties of copper matrix composites of reinforced with TiC particles, J. Alloys Compd. 676 (2016) 120–126.
[32] S. Panda, K. Dash, B.C. Ray, Processing and properties of Cu based micro- and nano- composites, Bull. Mater. Sci. 37 (2014) 227–238.
[33] S.C. Liao, W.E. Mayo, K.D. Pae, Theory of high pressure/low temperature sintering of bulk nanocrystalline TiO_2, Acta Mater. 45 (1997) 4027–4040.
[34] J.J. Ni, J. Li, W. Luo, Q. Han, Y.B. Yin, Z.F. Jia, B.X. Huang, C. Hu, Microstructure and properties of in-situ TiC reinforced copper nanocomposites fabricated via long-term ball milling and hot pressing, J. Alloys Compd. 755 (2018) 24–28.
[35] J. Li, J.J. Ni, B.X. Huang, J.X. Chen, Z.L. Xu, S.D. Liao, C.Z. Wang, W. Luo, Long-term ball milling and hot pressing of in-situ nanoscale tungsten carbides reinforced copper composite and its characterization, Mater. Charact. 152 (2019) 134–140.
[36] D. Nunes, V. Livramento, R. Mateus, J.B. Correia, L.C. Alves, M. Viarigues, P. A. Carvalho, Mechanical synthesis of copper-carbon nanocomposites: structural changes, strengthening and thermal stabilization, Mater. Sci. Eng. A 528 (2011) 8610–8620.
[37] A. Nieto, H. Yang, L. Jiang, J.M. Schoenung, Reinforcement size effects on the abrasive wear of boron carbide reinforced aluminum composites, Wear 390-391 (2017) 228–235.
[38] B. Sivaiah, M. Saravanan, D. Ajay, Nanoindentation and wear characteristics of Al5083/SiC_p nanocomposites synthesized by high energy ball milling and spark plasma sintering, J. Mater. Sci. Technol. 28 (2012) 969–975.

[39] J.L. Cabezas-Villa, L. Olmos, H.J. Vergara-Hernández, O. Jiménez, P. Garnica, D. Bouvard, M. Flores, Constrained sintering and wear properties of Cu-WC composites, T. Nonferr. Metal. Soc. 27 (2017) 2214–2224.
[40] S. Kumar, V. Balasubramanian, Effect of reinforcement size and volume fraction on the abrasive wear behaiour of AA7075 Al/SiC_p P/M composites-A statistical analysis, Tribol. Int. 43 (2010) 414–422.
[41] C.F. Miller, G.W. Simmons, R.P. Wei, High temperature oxidation of Nb, NbC and Ni_3Nb and oxygen enhanced crack growth, Scr. Mater. 42 (2000) 227–232.
[42] Y.Z. Zhan, G. Zhang, Mechanical mixing and wear-debris formation in the dry sliding wear of copper matrix composite, Tribol. Lett. 17 (2004) 581–592.
[43] G.H. Zhou, H.Y. Ding, Wear performance of alumina-reinforced copper-matrix composites prepared by powder metallurgy, J. Eng. Tribol. 227 (2013) 1011–1017.